Evaluation of Control Line Reefing Systems for Circular Parachutes

Article *in* Journal of Aircraft · February 2016

DOI: 10.2514/1.C033524

CITATIONS
12

READS
1,443

1 author:

Travis Fields
University of Missouri - Kansas City
47 PUBLICATIONS **163** CITATIONS

SEE PROFILE

Evaluation of Control Line Reefing Systems for Circular Parachutes

Travis D. Fields[1]
University of Missouri-Kansas City, Kansas City, Missouri, 64110, USA

I. Introduction

Aerial delivery operations provide supplies in areas and situations not reachable with any other supply method [1]; however, traditionally uncontrolled circular parachutes can only be accurately delivered from low altitudes. Several autonomous decelerator vehicle (ADV) techniques have been investigated to improve aerial delivery landing location accuracy. Small-scale high accuracy ram-air parafoil systems have seen tremendous success in landing accuracies with circular error probables (CEP) of approximately 10m [2–4]. Additionally, several alternative ram-air parafoil control techniques that reduce actuator requirements or improve accuracy have been developed and evaluated including glide slope control[5, 6], upper surface spoilers[7], and payload weight shift control[8]. **It is important to note that small-scale ram-air systems are typically more accurate than the full-scale counterparts.**

Although parafoil systems have demonstrated extremely high landing location accuracy in small-scale testing, full-scale parafoil systems are rarely used in combat scenarios because of the high system cost [1]. Ram-air systems are also incapable of producing zero glide slope in a wind-fixed frame, limiting applicability in urban environments and rough terrain environments [9]. To improve landing location accuracy over traditional uncontrolled aerial delivery techniques while minimizing the system cost, two different circular parachute control strategies have been evaluated; asymmetric and symmetric canopy deformation. Asymmetric canopy deformation provides rudimentary steering capabilities of the delivery system. Canopy deformation is achieved with four pneumatic muscle

---

[1] Assistant Professor, Civil and Mechanical Engineering, 5110 Rockhill Rd FH 352, and AIAA Member.

actuators or electromechanical actuators attached to the suspension lines [10–12]. Simulation results with actual atmospheric wind data have demonstrated sufficient accuracy (CEP $<$ 100 m); however, the required canopy and payload modifications and crew training requirements have limited the applicability of the asymmetric canopy deformation methods. Descent rate control is a less invasive ADV strategy that utilizes symmetric canopy deformation to control the vehicle descent speed in the presence of known atmospheric wind conditions. A simple, constant drag area approach has been developed in which the vehicle attempts to navigate to a target line segment (i.e. road) [13]. A more advanced path planning strategy was also developed to capitalize on the capability of the vehicle to modify the parachute size continuously during descent [14]. This time varying strategy enables the vehicle to "steer" towards a target point (rather than a line segment). Preliminary flight testing was performed with a prototype reversible reefing symmetric canopy deformation system coupled with a quarter-spherical cross-based canopy, where descent rate was controlled with an electromechanical reeling system [15]. The vehicle exhibited high descent speed controllability; however, the required reeling actuator force was equal to the entire payload weight (which may be problematic for heavy cargo systems). Additionally, high canopy-payload relative yaw motion was observed during testing with flat-circular canopies, thereby severely limiting the system applicability into current delivery operations.

In addition to terrestrial aerial delivery applications, symmetric canopy deformation also has significant potential for planetary reentry vehicles. Current reentry decelerator systems employ reefing systems to reduce the chance of parachute failure by reducing canopy inflation loads [16, 17]. Typical reefing practice incorporates reefing lines fixed to the canopy that reduce inflated size during parachute deployment. Time-based reefing cutters are used to cut the reefing line, allowing the canopy to inflate to the next reefing stage. The primary concern with time-based reefing cutters is the inability to adjust the timing schedule in real-time. The Orion parachute system was designed to withstand a single reefing stage failure during nominal reentry [18, 19]. **In a pad abort scenario the main canopies are deployed with extremely high dynamic pressure that could cause canopy failure [20]**. The inability to adjust the reefing stages can cause potentially catastrophic results when designed for one scenario (i.e. nominal reentry deployment), and are activated in

another scenario (i.e. aborted mission deployment).

To increase efficiency and applicability of descent rate control strategies, several new reefing techniques were tested. In total, three reefing techniques were tested and compared to the previously developed reeling-based reefing effort. The three reefing strategies stemmed from a single control-line approach in which a single control line can manipulate the parachute size/shape directly while theoretically carrying only a small portion of the suspension line load (which was identified as one of the two major limitations of the reel-based reefing methodology tested previously). The continuous control line-based skirt reefing methodology was originally noted by Knacke [17] and was later implemented by Sadeck and Lee [21]. It is important to note these continuous reefing systems were developed for **open loop control-based** continuous disreef capabilities only, not for reversible reefing of a parachute canopy. The focus of this study is on the development and testing of a control line-based continuous reversible reefing systems similar to the system noted by Knacke.

II. Methodology

A. Reefing Techniques

In this study four different reefing techniques were evaluated as shown in Figure 1. Center loop control line reefing (Figure 1 (a)) requires small lines to be fixed to the canopy skirt at the suspension line/skirt attachment point. These small lines are then attached to a single control line, which when actuated, forces the skirt closed. The reefing lines are approximately the length of the canopy radius when fully inflated. **In an attempt to keep the reefing lines approximately perpendicular to the canopy regardless of the reefing amount, a second method incorporating a small guide ring attached to the canopy (Figure 1 (b)) was created for evaluation.** A two loop control line technique (Figure 1 (c)) incorporates two loops woven through the suspension line attachment points and connected to a single control line in the center of the canopy. During control line actuation, the two loops constricts the canopy in a manner similar to a bag drawstring system. Finally, the suspension line reefing technique (Figure 1 (d)) uses a winch actuator to reel all of the suspension lines to achieve the desired descent speed. It is important to note that for each reefing technique, the configuration/setup was adjusted to provide the best

possible results with the given hardware prior to final data collection.

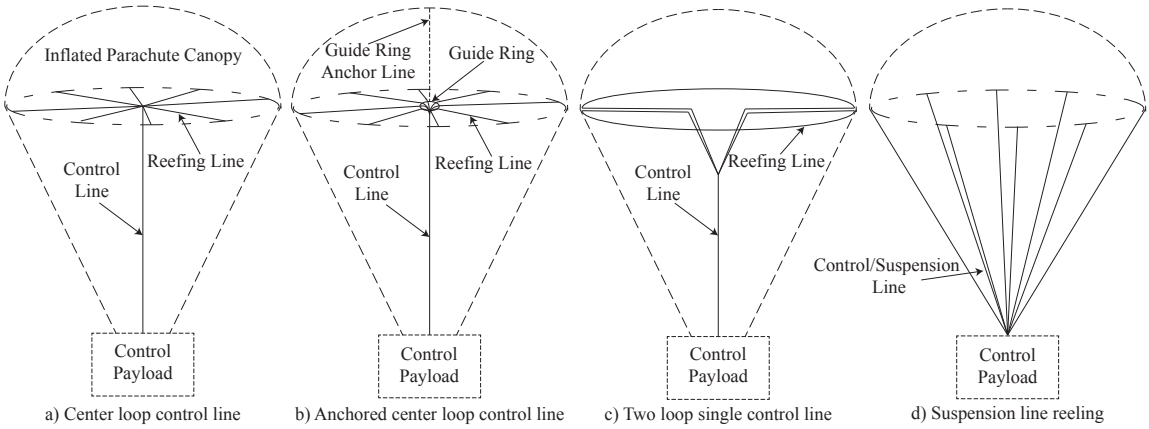

Fig. 1: The four different types of reefing techniques evaluated, where solid lines indicate control and/or reefing lines.

The payload contains an Arduino microcontroller with onboard inertial measurement unit and barometric pressure transducer (MultiWii), electric winch servomotor, miniature load cell, and a 2.4 GHz remote control receiver (typically used for hobbyist aircraft). The Arduino microcontroller receives all commands from the R/C receiver, transmits angular position commands to the servomotor, and stores all data to a SD card logger. Time, altitude, control line load, and servo position data were collected and stored at a sampling rate of approximately 30 Hz. The total payload mass with added ballast weight is 2.1 kg.

A miniature load cell was attached to the control line for each of the techniques tested in order to quantify the actuation force needed for each configuration. The average load (at terminal velocity) and the maximum load experienced during flight testing were reported for each reefing level. The reported control line loads provide an estimate of the steady state actuator force required as well as an indication of actuator/payload peak loading requirements. For the reeling-based reefing technique (Figure 1 (d)) the actuation force is simply the weight of the payload; therefore, the load cell was not incorporated into the reeling-based reefing system. The load cell was connected to a custom instrumentation amplifier printed circuit board (PCB). The PCB output voltage range was $0-5$ V, which can be more accurately sampled with the $0-5$ V 10-bit A/D converter onboard the microcontroller. The output range of the PCB correlates directly with a tension load of $0-33$ N

$(0 - 7.4$ lbs). Calibration was performed with standard calibration techniques [22, 23] with the use of a Bose ElectroForce load frame.

B. Testing Method

Drop testing was conducted with a scaled flat-circular 1.2m (4.0 ft) canopy with a payload mass of 2.1 kg (4.6 lbs). A guide-line was used during testing to minimize canopy-payload relative rotation, and provide repeatable results. The top of the guide line was fixed to a a semi-rigid anchor system mounted in a large indoor environment, producing a drop height of 13.2m (43.3ft). The bottom of the guide-line was fixed to the structure floor by attaching the guide-line to a large set of free weights. The testing environment cross section is 6.1m x 6.1m (20ft x 20ft), resulting in a blockage ratio of approximately 3% which is similar to the blockage ratio encountered by other indoor parachute testing programs. **Desabrais *et al* reports use of up to 9 ft canopies in a 100ft diameter testing facility ($\approx 1\%$ blockage) that incorporated a 120 ft long guide line [24]. An illustration of the drop system used for the small-scale testing regime described herein is shown in Figure 2.**

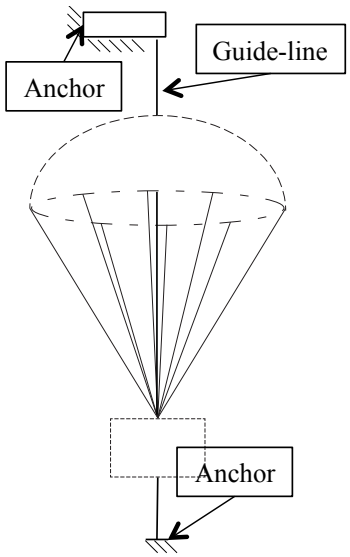

Fig. 2: Indoor guide-line drop testing apparatus illustration.

Due to the relatively low drop altitude, the reefing level was fixed during each test. Multiple drops were performed at each reefing level to quantify the variability in the descent rate, with a minimum of two drops performed at each reefing level. The number of discrete reefing values tested

varied depending on the specific configuration, with ten, nine, seven, and five reefing levels tested for configurations A, B, C, and D, respectively. **The zero reefing condition was qualitatively estimated by decreasing reefing amount until the canopy was fully inflated during descent. Full reefing was then defined as a 0.42 m (1.4 ft) control line/suspension line contraction from the zero-reefing condition. All four configurations were evaluated with an identical control line deflection range (0 - 0.42 m). Because of the qualitative zero-reef condition, a particular configuration may be biased. However, the bias has negligible impact on the overall conclusions of the study as the resulting controllable descent speed range will be nearly identical as the unbiased case.** By performing only static reefing testing, the dynamic reefing load cannot be quantified; however, the change in reefing load during dynamic reefing will vary only slightly from the static case. This of course depends on the speed of the reefing actuator, but a limited amount of dynamic flight testing, **particularly with configurations A and C,** has shown the reefing actuator used in this study is capable of transitioning from full to zero reefing in approximately two seconds, resulting in only small ($< 15\%$) increases in the terminal control line load. As mentioned previously, the control line loading data reported in this study are estimated from **both the average control line load at terminal velocity and** the maximum control line load experienced during the drop test.

The measured flight data was used to calculate the descent speed and control line force at various reefing levels (or servo positions) for each of the tested reefing techniques. The barometric altimeter data was used to estimate the descent speed via numerical differentiation. To reduce differentiation induced noise, a moving five point linear least-squares trend line was used to estimate the descent speed. The resulting slope of the linear trend line at each time interval was stored as the estimated descent speed. An example of a single drop test in the fully open (zero reef) and fully closed (fully reefed) setting for configuration C is shown in Figure 3. Although the drop time is short, the **canopy appears to approach terminal velocity prior to reaching the ground as indicated by the speed (particularly the zero reef-scenario) approaching a constant descent speed of approximately** 6 **m/s. It is important to note that only the segments of quasi-constant descent speed are used for this study (i.e. approximately 1.4 - 1.9 s**

in Figure 3). At least six descent speed and control line load estimates are used to calculate the average descent speed and average control line load; however, with slower descents the number of data points used is typically $\approx 15-20$. Although the fully-reefed drop test may not reach terminal velocity prior to impact, the reported descent speed ranges will be more conservative estimates of the actual achievable descent ranges in full-scale testing. **Due to the short test durations, canopy oscillations (breathing) are not visible which will slightly degrade canopy descent speed estimates.** An instrument uncertainty analysis (95 % confidence) yielded an estimated uncertainty in descent speed (based on altitude and time measurements) of ± 0.21 m/s (0.69 ft/s). The expected speed range of each technique is approximately $5.0-9.5$ m/s $(16-31$ ft/s), resulting in a maximum relative uncertainty (occurs at the slowest descent speed) of 4.2%. Similarly, the load cell instrument uncertainty (95% confidence) was found to be ± 0.040 N (± 0.0090 lbs) based on collected calibration data. It is important to note that the reported uncertainties are for the measurement only, and do not include uncertainties induced by the experiment technique itself.

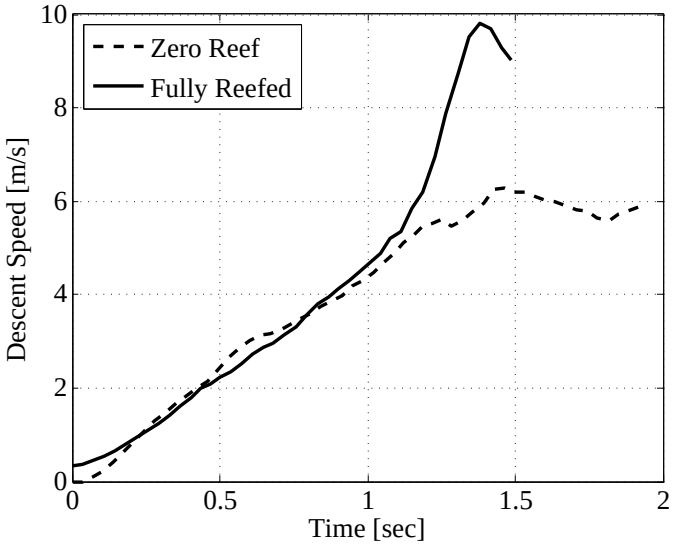

Fig. 3: Velocity data collected from fully open reefing level for configuration C.

III. Results

In total, 74 fixed mass drop tests were performed spanning all four parachute configurations. For each configuration 5-10 different reefing values were tested, with 2-4 drop tests conducted at each reefing value. Testing was conducted with nearly identical atmospheric conditions (both tem-

perature and pressure) for the 74 drop tests. **A representative drop test (zero reef condition) including both descent speed and control line load for configurations A and C are shown in Figures 4 and 5, respectively. The average descent speed at terminal velocity and average control line load for the representative configuration A drop test was estimated from the time range of 1.5 - 2.0 s. For the representative configuration C test, the average descent speed and control line load were estimated from time range of 1.5 - 2.2 s.**

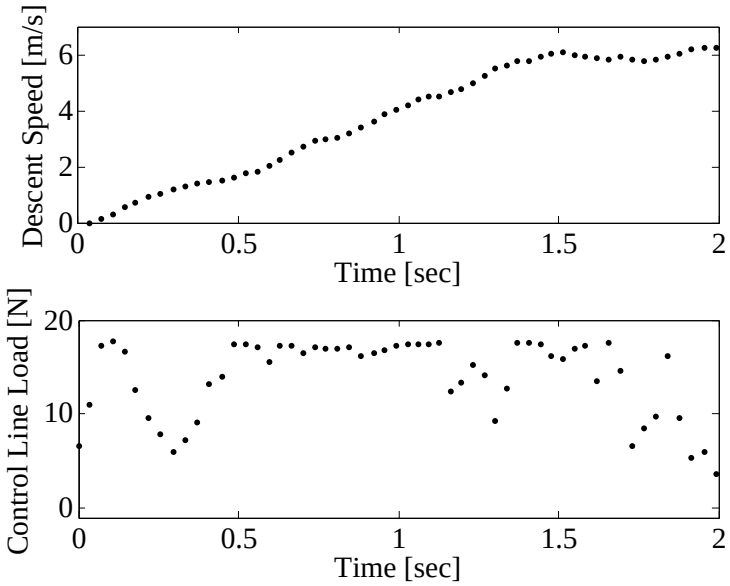

Fig. 4: Zero reefed configuration A drop test including descent speed and control line load after release.

The resulting terminal descent speed at each reefing level for the four parachute configurations are shown in Figure 6. **For each configuration, a linear fit was applied to the data to improve clarity. A third order polynomial could also be applied to capture reefing saturation near the minimum and maximum reefing values.** Configuration A had the slowest overall descent speed, with a speed range of $4.6-6.5$ m/s ($15.1-21.3$ ft/s) which corresponds to a percent increase of 41% in descent speed relative to the fully open configuration. Descent speed results for the each configuration are tabulated in Table 1. Configuration D produced the largest controllable range of decent speeds, with configuration A producing the smallest controllable range.

To investigate the actuator force required to maintain the different levels of reefing with the four

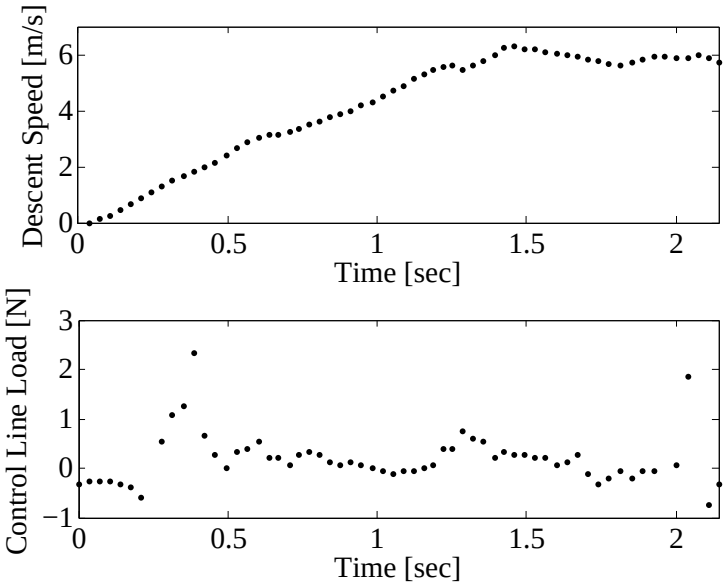

Fig. 5: Zero reefed configuration C drop test including descent speed and control line load after release.

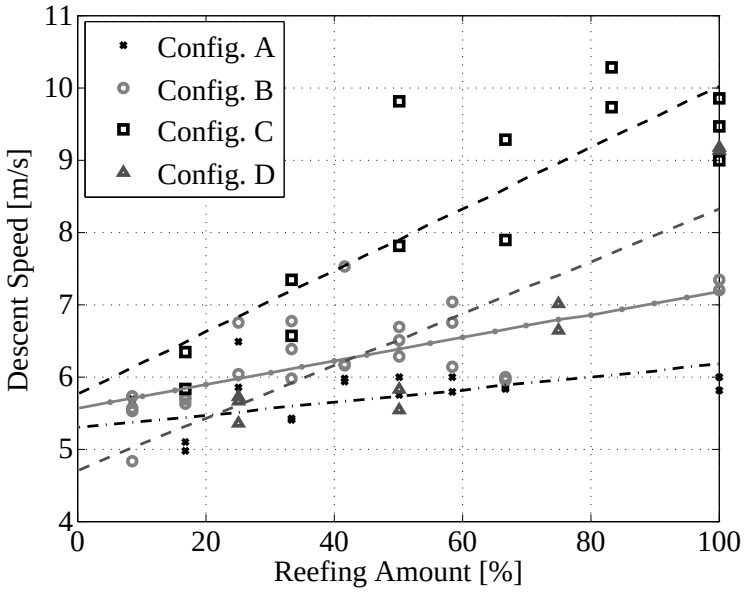

Fig. 6: Average descent speed for the four tested parachute configurations at various levels of reefing with drop height of 13.2 m and payload mass of 2.1 kg.

configurations, a load cell was fixed to the control line. For configuration D, no load cell was used as the actuator force required is equal to the weight of the payload. Figure 7 provides the average control line load near terminal velocity measured during a flight test at each of the static reefing levels. **For configuration C, the peak load typically occurred near the time of inflation.**

Table 1: Speed range and percentage increase for each parachute configuration

Reefing Configuration	Speed Range [m/s]	% Speed Increase [%]
A	$4.6 - 6.5$	41
B	$4.8 - 7.5$	56
C	$5.5 - 10.3$	87
D	$4.9 - 9.2$	88

As the amount of reefing increases, the size of the peak relative to the steady state load decreases (steady state load increases as reefing increases). For configurations A and B, the peak load also tends to occur near inflation; however, the size of the peak relative to the steady state load is quite small ($\approx 1 - 2N$). The peak control line load was measured to be 18.6 N (4.17 lbs), 19.1 N (4.28 lbs), 2.50 N (0.56 lbs), and 20.4 N (4.57 lbs) for configurations A, B, C, and D, respectively.

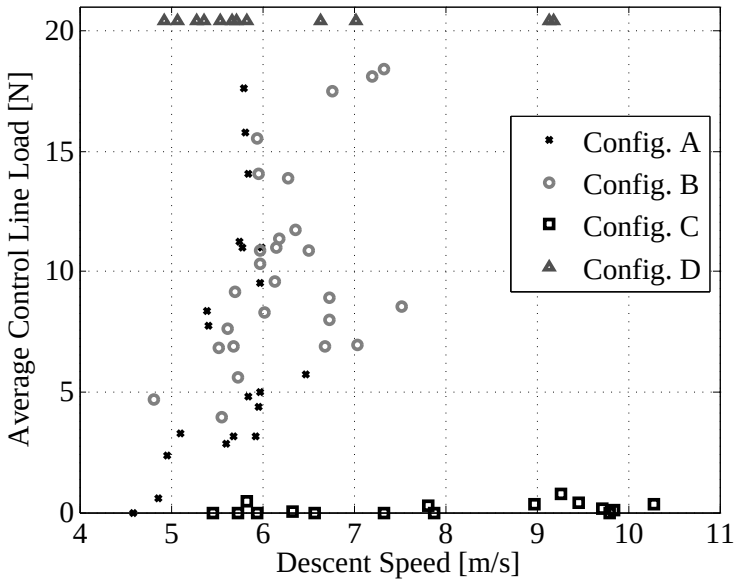

Fig. 7: Average control line load experienced at various reefing levels for the four tested parachute configurations with drop height of 13.2 m and payload mass of 2.1 kg.

IV. Discussion

The drop testing results indicate that both configurations A and B do not provide sufficiently large descent control ranges and require significant actuator forces. The controllability for both methods was substantially lower than the other two configurations evaluated, limiting applicability in descent strategies that rely heavily on descent speed changes (such as the asymmetric deformation technique). The guide ring provided only minimal increase in descent speed controllability; however, the installation costs for the added ring severely outweigh the small increase in control. Compared to configurations C (two loop control line reefing) and D (reeling-based reefing), configurations A and B required significant canopy reconfigurations (for attachments of the reefing lines) prior to testing. Additionally, the added canopy-payload complexity introduced safety considerations due to excessive suspension line, reefing line, and control line tangling during descent. Configuration B was particularly prone to tangling, as the ring mounted near the canopy apex tended to tangle with suspension lines during canopy inflation.

The poor performance of the the two configurations can be attributed to the geometry of the individual reefing lines attached at the suspension line/canopy confluence point. As the control line is shortened, the angle of the reefing lines relative to the canopy suspension lines, θ, quickly approaches zero (Figure 8). As θ decreases, the control line takes more of the payload weight until the entire payload weight is carried only by the control line. Drop test results indicate at full reef the control line load approaches $\approx 85\%$ of the payload weight. The individual reefing lines also do not provide sufficient inward force as the lines are nearly vertical during reefing, severely limiting the reduction in parachute wetted area. The ring added for configuration B was intended to reduce these limitations; however, the resulting system produced severe rigging complications, namely the line tangling issue mentioned previously as well as the loading applied to the apex of the canopy. These results provide insight into the deficiencies of the center loop control line reefing techniques.

The descent range achieved with the reel-based reefing technique (configuration D) correlate well with previous reeling-based reefing autonomous decelerator vehicle flight results [15] (measured descent speed range of $5 - 10$ m/s) applied to a quarter-spherical cross-based canopy as opposed to a flat-circular canopy. Reeling-based reversible reefing clearly provides tremendous descent speed

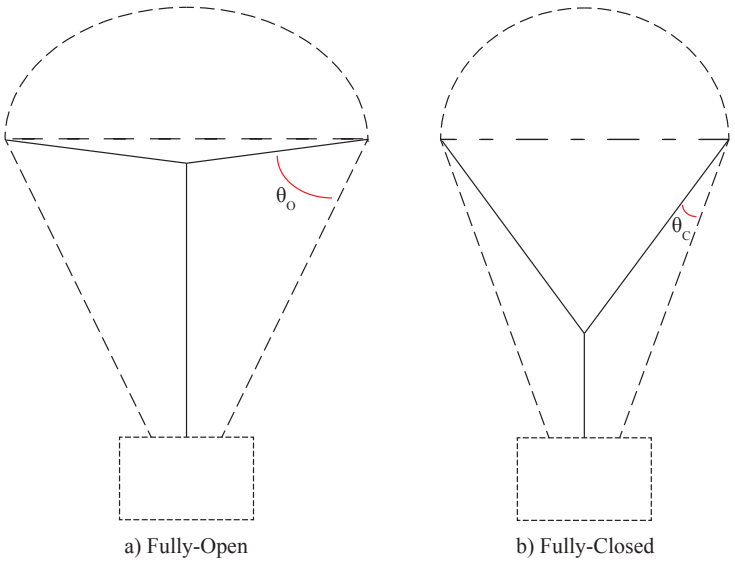

Fig. 8: Fully-open and fully-closed reefing level for configuration A

control; however, regardless of the hardware, the actuator must be capable of lifting the entire payload weight. For small-scale systems this limitation may be negligible, but when attempting to implement such a system at full-scale the actuator requirements quickly prove impractical. The focus of this study was on the evaluation of reefing methods compared to the reeling-based approach, but it is important to note the similarity in controllable range between the larger scale study, and the measured range with the small-scale system. The similarity provides some confidence in the scalability of the reeling-based approach, permitting comparisons between the other small-scale reefing techniques tested.

Configuration C outperformed all other configurations tested, resulting in significantly lower control line load and high descent speed controllable range. As expected, the required actuator load (measured on the control line) increases with the amount of reefing (and correspondingly increased descent speed), but even the maximum required actuator load of 2.5 N is only $\approx 12\%$ of the payload weight. It is important to note that when analyzing the examining the average control line loads, the actuator requirements are only $\approx 5\%$ of the payload weight. Scaling this system to a full size parachute/payload system, the actuator would be substantially smaller than the reeling-based technique counterpart. The level of reefing is also approximately linearly proportional to the change in descent speed, resulting an in ideal control mechanism for use in autonomous decelerator vehicles. Compared to the reeling-based reefing technique, the single control line approach can

also be modified to reduce the control line deflection necessary to fully reef the canopy. This is particularly evident with canopies attached to long suspension lines, as the reeling-based technique must reel in the entire suspension line to fully reef the canopy. The double loop reefing technique requires control line displacement equal to approximately the canopy diameter, and can be further reduced by implementing a four (or more) loop system.

It is important to note that for this study the stability of the various configurations was not fully evaluated. With the limited drop height used in this study, the steady state behavior could not be completely captured. Therefore, a stability analysis of configuration C should be conducted prior to implementation of such a system. The time history data does provide some conservative confidence in the results; however, particular attention must be paid to the relative canopy-payload rotation that can occur during full canopy reefing. The relative rotation can cause significant suspension line tangling, which when later disreefed may prevent canopy inflation from occurring. Although this type of behavior was not seen during flight testing, similar testing should be conducted with the control line reefing technique to ensure stable canopy reefing and disreefing to ensure a stable reversible reefing prior to implementation.

V. Conclusion

Reversible reefing has potential for both autonomous descent vehicles and atmospheric reentry vehicles; however, a practical reversible reefing technique has not been developed. To evaluate four reversible reefing techniques, a payload was constructed which measured the payload motion and the control line force via miniature load cell. Data was collected onboard the payload, and stored for post-processing upon test completion. From the four reefing candidates identified in the study, configuration C (double loop control line reefing) required very small actuation forces (12% payload weight *maximum*) to maintain canopy shape throughout the various levels of reefing. Additionally, configuration C had approximately the same controllable descent speed range as the only previously developed reeling-based reversible reefing technique (configuration D). Flight testing of configuration C demonstrated a high level of linearity between the level of reefing and the corresponding descent speed for two different payload weights, resulting an ideal candidate for use in ADV path

planning strategies.

VI. Acknowledgements

This research was funded by the University of Missouri-Kansas City Summer Undergraduate Research Opportunity Program (SUROP). The author would like to acknowledge Aldair Gongora, Nicolas Basore, John Bazin, and Daniel Schroeder for their assistance during drop testing and prototype development.

References

[1] Benney, R., "History and Challenges of Airdrops in Afghanistan-Invited Lecture," in "22nd AIAA Aerodynamic Decelerator Systems Conference and Seminar," , Daytona Beach, Florida, March 25-28, 2013.

[2] Slegers, N. J., Rogers, J., and Brown, A., "Experimental Investigation of Stochastic Parafoil Guidance Using a Graphic Processing Unit," in "23rd Aerodynamic Decelerator Systems Technology Conference and Seminar," , Daytona Beach, Florida, March 30 - April 2, 2015, AIAA Paper 2015-2106.

[3] Slegers, N. and Rogers, J., "Terminal Guidance for Complex Drop Zones Using Massively Parallel Processing," in "22nd AIAA Aerodynamic Decelerator Systems Conference and Seminar," , Daytona Beach, Florida, March 25-28, 2013, AIAA Paper 2013-1343.

[4] Slegers, N., "Effects of Canopy-Payload Relative Motion on Control of Autonomous Parafoils," *Journal of Guidance, Control, and Dynamics*, Vol. 33, No. 1, 2010, pp. 116–125, doi: 10.2514/1.44564.

[5] Slegers, N., Beyer, E., and Costello, M., "Use of Variable Incidence Angle for Glide Slope Control of Autonomous Parafoils," *Journal of Guidance, Control and Dynamics*, Vol. 31, No. 3, 2008, pp. 585–596, doi: 10.2514/1.32099.

[6] Ward, M., Gavrilovski, A., and Costello, M., "Flight Test Results for Glide Slope Control of Parafoil Canopies of Various Aspect Ratios," in "21st AIAA Aerodynamic Decelerator Systems Conference and Seminar," , Dublin, Ireland, May 23-26, 2011, AIAA Paper 2011-2620.

[7] Ward, M. and Costello, M., "Autonomous Control of Parafoils Using Upper Surface Spoilers," in "22nd AIAA Aerodynamic Decelerator Systems Conference and Seminar," , Daytona Beach, Florida, March 25-28, 2013, AIAA Paper 2013-1379.

[8] Ward, M., Culpepper, S., and Costello, M., "Parafoil Control Using Payload Weight Shift," *Journal of Aircraft*, Vol. 51, No. 1, 2014, pp. 204–215, doi:10.2514/1.C032251.

[9] Benney, R., "An Overview of DoD Aerial Delivery Capabilities and Needs-Invited Lecture," in "23rd Aerodynamic Decelerator Systems Technology Conference and Seminar," , Daytona Beach, Florida, March 30 - April 2, 2015.

[10] Benney, R., Brown, G., and Stein, K., "A New Pneumatic PMA: Its Use in Airdrop Applications," *AIAA Paper 2001-2022*.

[11] Dobrokhodov, V. N., Yakimenko, O. A., and Junge, C. J., "Six-Degree-of-Freedom Model of a Controlled Circular Parachute," *Journal of Aircraft*, Vol. 40, No. 3, 2003, pp. 482–493, doi: 10.2514/6.2002–4613.

[12] Yakimenko, O. A., Dobrokhodov, V. N., and Kaminer, I. I., "Synthesis of Optimal Control and Flight Testing of an Autonomous Circular Parachute," *Journal of Guidance, Control, and Dynamics*, Vol. 27, No. 1, 2004, pp. 29–40, doi: 10.2514/1.9282.

[13] Fields, T. D., LaCombe, J. C., and Wang, E. L., "Autonomous Guidance of a Circular Parachute Using Descent Rate Control," *Journal of Guidance, Control, and Dynamics*, Vol. 35, No. 4, 2012, pp. 1367–1370, doi: 10.2514/1.55919.

[14] Fields, T. D., LaCombe, J. C., and Wang, E. L., "Time Varying Descent Rate Control Strategy for Circular Parachutes," *Journal of Guidance, Control and Dynamics*, Vol. 38, No. 8, 2015, pp. 1468 – 1477, doi: 10.2514/1.G000627.

[15] Fields, T. D., LaCombe, J. C., and Wang, E. L., "Flight Testing of a 1-DOF Variable Drag Autonomous Descent Vehicle," in "22nd AIAA Aerodynamic Decelerator Systems Technology Conference and Seminar," , Daytona Beach, FL, March 25-28, 2013, AIAA Paper 2013-1377.

[16] Ray, E. S., "Reefing Line Tension in CPAS Main Parachute Clusters," in "22nd AIAA Aerodynamic Decelerator Systems Conference and Seminar," , Daytona Beach, Florida, March 25-28, 2013, AIAA Paper 2013-1393.

[17] Knacke, T., *Parachute Recovery Systems Design Manual*, Para Publishing, first edition ed., 1992.

[18] Ray, E. S., "Reconstruction of Orion EDU Parachute Inflation Loads," in "22nd AIAA Aerodynamic Decelerator Systems Conference and Seminar," , March 25-28, 2013, Daytona Beach, Florida, AIAA Paper 2013-1260.

[19] Takizawa, K., Tezduyar, T. E., Boswell, C., Kolesar, R., and Montel, K., "FSI modeling of the reefed stages and disreefing of the Orion spacecraft parachutes," *Computational Mechanics*, Vol. 5, No. 54, 2014, pp. 1203–1220, DOI: 10.1007/s00466–014–1052–y.

[20] Lichodziejewski, D., Taylor, A. P., Sinclair, R., Olmstead, R., Kelley, C., Johnson, J., Melgares, M., Morris, A., and Bledsoe, K., "Development and Testing of the Orion CEV Parachute Assembly System (CPAS)," in "20th AIAA Aerodynamic Decelerator Systems Technology Conference and Seminar," ,

May 4-7, 2009, Seattle, Washington, AIAA Paper 2009-2938.

[21] Sadeck, J. E. and Lee, C. K., "Continuous Disreefing Method for Parachute Opening," *Journal of Aircraft*, Vol. 46, No. 2, 2009, pp. 501–504, doi: 10.2514/1.37444.

[22] Anderson, G. B. and Raybold, R. C., "Studies of Calibration Procedures for Load Cells and Proving Rings as Weighing Devices," *National Bureau of Standards*.

[23] "Procedure for Calibrating Force Transducers (Load Cells)," Tech. rep., United States Department of the Interior Bureau of Reclamation, 1989, USBR Paper No. 1045-89.

[24] Desabrais, K. J., Lee, C. K., Buckley, J., and Jones, T. W., "Experimental Parachute Validation Research Program and Status Report on Indoor Drop Tests," *19th AIAA Aerodynamic Decelerator Systems Technology Conference and Seminar*.